J. Fluid Mech. (2005), *vol.* 545, *pp.* 281–289.
doi:10.1017/S0022112005007147 Printed in the United Kingdom

Crossflow instability in rotor–stator flows with axial inward throughflow

By S. PONCET AND M.-P. CHAUVE

IRPHE, UMR 6594, CNRS- Universités d'Aix-Marseille I & II, Technopôle Château-Gombert, 49, rue F. Joliot-Curie, 13384 Marseille cédex 13, France

(Received 20 May 2005 and in revised form 6 September 2005)

From visualizations and velocity measurements, we study the formation of new spiral patterns at the periphery of a rotor–stator cavity when an axial inward throughflow is superimposed. We determine the transition diagram for a given intermediate aspect ratio in the plane (Re, V_z), where Re is the rotational Reynolds number and V_z the axial velocity in the radial gap between the rotating disk and the shroud. Both techniques are used to characterize the frequency, the azimuthal wavenumber, the inclination angle of the spirals and to localize them axially and radially. We also show that this new instability is a crossflow instability due to the strong competition between rotation and throughflow.

1. Introduction

Rotating disk flows are not only a subject of academic interest as a model geometry to study how rotation influences turbulence but have also a major application in turbomachinery. Numerous recent experimental (Gauthier, Gondret & Rabaud 1999; Schouvelier, Le Gal & Chauve 2001; Cros & Le Gal 2002) and numerical (Cousin-Rittemard, Daube & Le Quéré 1998; Serre, Crespo del Arco & Bontoux 2001) studies have been devoted to instabilities in rotating flows. In a closed rotor-stator cavity of large aspect ratio $G = h/R \geqslant 7.14 \times 10^{-2}$ (h the interdisk space and R the disk radius), the first instability, which appears by increasing the rotating disk speed, is a viscous instability, which develops in the stator boundary layer (the Bödewadt layer) and consists of circular rolls travelling through the centre of the cavity. On increasing the Reynolds number, a second bifurcation leads to the development of a system of spiral rolls denoted SR1 located at the periphery of the cavity. They are characterized by a positive orientation angle $\epsilon \simeq 25^\circ$ with the tangential direction. The angle ϵ is counted positive when spirals are rolled up towards the disk axis in the rotation sense of the rotor. When the Reynolds number is further increased, the flow results from the coexistence of these two modes. For intermediate values of the aspect ratio in the range $1.79 \times 10^{-2} \leqslant G < 7.14 \times 10^{-2}$, Schouvelier *et al.* (2001) have observed another instability, which consists again of a network of spiral rolls denoted SR2 ($12^\circ \leqslant \epsilon \leqslant 15^\circ$). For lower aspect ratios, the flow is of torsional Couette type with joined boundary layers. Cros & Le Gal (2002) have investigated the transition from laminar to turbulent states for this kind of flow. By increasing the Reynolds number, they observed three different bifurcations starting from spiral rolls denoted SR3 ($-5^\circ \leqslant \epsilon \leqslant -3^\circ$), solitary waves and turbulent spots.

To our knowledge, the only study concerning the instabilities occurring in a rotor-stator cavity when a centripetal throughflow is superimposed has been performed

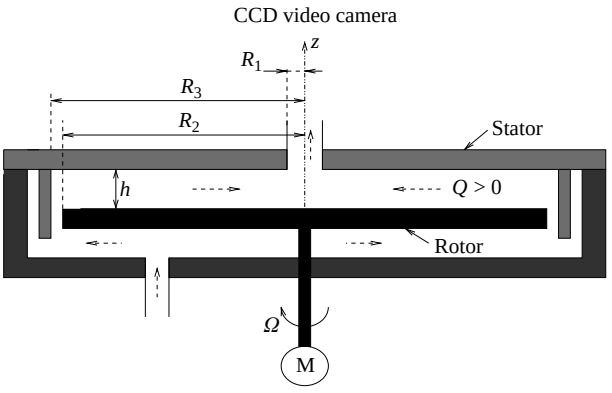

FIGURE 1. Schematic diagram of the experimental rig with relevant notation.

recently by Rémy (2004) using stereoscopic particle image velocimetry (PIV) and Rémy, Gauthier & Buisine (2005) using a tomography technique. They have studied the SR1 spiral rolls in a rotor-stator system with suction for large aspect ratios $G \geqslant 0.088$. When the flow rate is increased, the thresholds of appearance and disappearance of these patterns decrease rapidly. They have also observed a crossflow instability, which takes place in the boundary layer of the cylindrical wall. This crossflow instability has been confirmed by the stability analysis of Rémy (2004).

The aim of this work is to extend the known results determined in the case of a closed cavity (Schouvelier *et al.* 2001) by introducing a flow-rate velocity as a new parameter and to study its effect on the thresholds of appearance and disappearance of the spiral structures SR2 and especially on the formation of new spiral rolls denoted SRJ2, which are due to the combination of both rotation and throughflow effects.

2. Experimental set-up

A sketch of the cavity is presented in figure 1. It consists of a smooth rotating disk (the rotor) of radius $R_2 = 140\,\text{mm}$ and a smooth fixed disk (the stator) enclosed by a fixed cylinder (the shroud) of radius slightly larger than the rotor $R_3 = 140.85\,\text{mm}$. The interdisk space h can vary between 0 and $21 \pm 0.02\,\text{mm}$. The two gaps at the outlet $R_1 = 10\,\text{mm}$ and the inlet $j = R_3 - R_2 = 0.85 \pm 0.025\,\text{mm}$ of the cavity enable an axial inward throughflow $Q > 0$ up to 240 l/h (the experimental limitation) to be superimposed. The water is contained in a lower tank and pumped to an upper one situated 3 m above the rotor-stator cavity. By using several concentric tanks, the fluid enters the experimental chamber by gravity to avoid any parasitical disturbance. Then the throughflow Q is adjusted by a flowmeter. Another parameter is the rate of rotation Ω of the rotating disk. It rotates at an uniform angular velocity Ω varying between 0 and $200\,\text{rad}\,\text{s}^{-1}$ with an accuracy of 0.2 %.

The cavity is filled with water maintained at a constant working temperature 20°C (kinematic viscosity of water $\nu \simeq 10^{-6}\,\text{m}^2\,\text{s}^{-1}$). In order to visualize the hydrodynamic structures, which develop in the flow during the transition from laminar to turbulent states, the water is seeded with reflective anisotropic particles of 'kalliroscope' (size $30 \times 6 \times 0.07\,\mu\text{m}$) in suspension, whose orientation depends upon the shear stress of the flow. The stator is a 20 mm thick Plexiglas plate, so that the flow can be observed through it. We illuminate the flow with an annular neon light and the surface of the

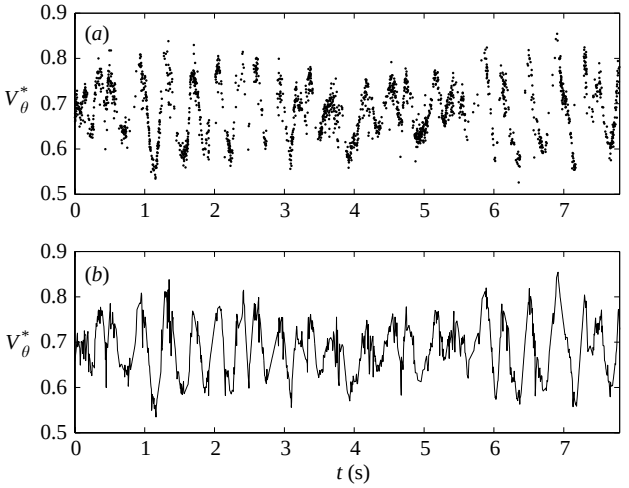

FIGURE 2. Temporal evolution of the tangential velocity for $Re = 2.05 \times 10^4$ and $V_z = 0.0754$ at ($r^* = 0.964$, $z^* = 0.567$): (*a*) rough signal, (*b*) resampled signal.

stainless steel rotor is painted black to improve the visualizations. Images (768×576 pixels) are taken at a video frequency of 25 images per second using a CCD video camera situated 1 m above the fixed disk.

We also performed velocity measurements by means of a two-component laser Doppler anemometer (LDA). This non-intrusive method is used to measure, from above the stator, the mean tangential V_θ and radial V_r velocity components in the vertical plane (r, z) at a given azimuthal angle. The seeding particles are the same for both techniques (no influence of these type of flakes is found for small rates of rotation).

The aim is to compare the frequency of the structures with the results obtained from visualizations. In figure 2(*a*), we represent the rough signal (6×10^4 points) of the tangential velocity component $V_\theta^* = V_\theta/(\Omega r)$ versus the time t at the point ($r^* = r/R_2 = 0.964$, $z^* = z/h = 0.567$) and for $Re = 2.05 \times 10^4$ and $V_z = 0.0754$. Note the periodicity of the signal: the high frequency corresponds in fact to the passage of the SRJ2 spirals. The signal is then resampled (figure 2*b*) using a first-order interpolation method (Piétry 1997). We choose the mean passing frequency of the particles as the resample frequency. From the resampled signal, we calculate the power spectral density DSP of the LDA data according to the frequency N (Hz).

3. Stability diagram for the aspect ratio $G = 0.0429$

The flow is mainly controlled by three parameters: the aspect ratio of the cavity $G = h/R_2$, the rotational Reynolds number $Re = \Omega R_2^2/\nu$ based on the rotating disk radius, and the mean axial velocity $V_z = Q/(2\pi j R_2)\,(\mathrm{m\,s^{-1}})$ in the radial gap at the inlet of the cavity under the assumption that j is small compared to R_2 (that is the case in the present study). The radial $r^* = r/R_2$ and axial $z^* = z/h$ locations are also two important local parameters to characterize instabilities in open rotor-stator flows. The aspect ratio is fixed at an intermediate value $G = 0.0429$ ($h = 6$ mm), for which the basic flow is of mixed type: a Batchelor type of flow pattern with separated boundary layers above a critical radius and a torsional Couette type of flow pattern with joined boundary layers below (Schouvelier *et al.* 2001). We recall that, for such

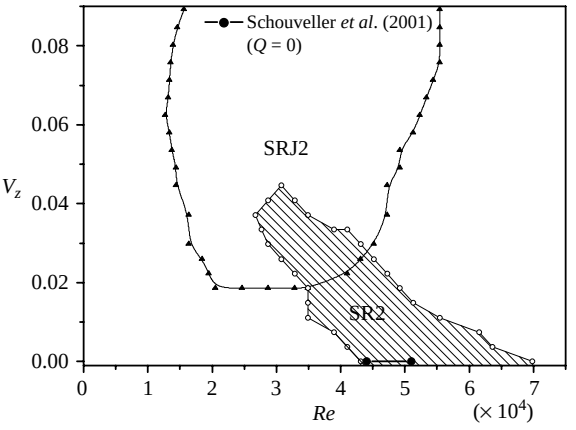

FIGURE 3. Stability diagram in the (Re,V_z) plane for the aspect ratio $G = 0.0429$.

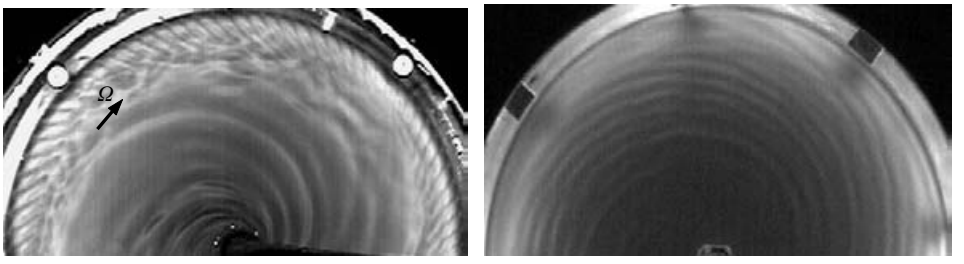

(*a*) (*b*)

FIGURE 4. Visualization of the spiral patterns (*a*) SRJ2 for $Re = 2.05 \times 10^4$ and $V_z = 0.0754$, (*b*) SR2 or $Re = 5.13 \times 10^4$ and $V_z = 0.0074$.

an aspect ratio, Schouvelier *et al.* (2001) observed two kinds of spiral rolls, denoted SR1 and SR2, which can coexist.

The transition diagram for the centripetal flow inside a rotor-stator cavity of aspect ratio $G = 0.0429$ is represented in figure 3 in the (Re,V_z)-plane. For example, for a given axial velocity $V_z = 0.03\ \mathrm{m\,s^{-1}}$, the basic flow is stable and loses its stability above a first threshold $Re \simeq 1.64 \times 10^4$. This leads to the formation of spiral rolls SRJ2 (figure 4*a*) located at the periphery of the cavity and which will be studied in more detail in the next section. From a second threshold $Re \simeq 2.89 \times 10^4$, a second bifurcation occurs and SR2 spiral rolls develop for $r^* < r_c^*$, where $r_c^* = r_c/R_2$ is the critical radius, above which the SRJ2 structures appear. For given Reynolds number and axial velocity, both instabilities can coexist but have respectively their own extended radial domain. For $4.29 \times 10^4 \leqslant Re \leqslant 4.52 \times 10^4$, though the flow is turbulent for a broad band of radius, the SRJ2 spirals exist at the periphery of the cavity but are quite difficult to observe, when the Reynolds number is increased. Above this last threshold, the flow is totally turbulent.

The SR2 spiral rolls (figure 4*b*) have been studied in detail by Schouvelier *et al.* (2001). The axes of these structures have a positive angle ϵ with the azimuthal direction: $12^\circ \leqslant \epsilon \leqslant 15^\circ$. Their network is stationary in the reference frame of the laboratory and occupies the whole cavity. In the case of a closed cavity ($V_z = 0$), the appearance threshold of the SR2 spirals is in excellent agreement with the one obtained by Schouvelier *et al.* (2001): $Re \simeq 4.4 \times 10^4$. On the other hand, there is a

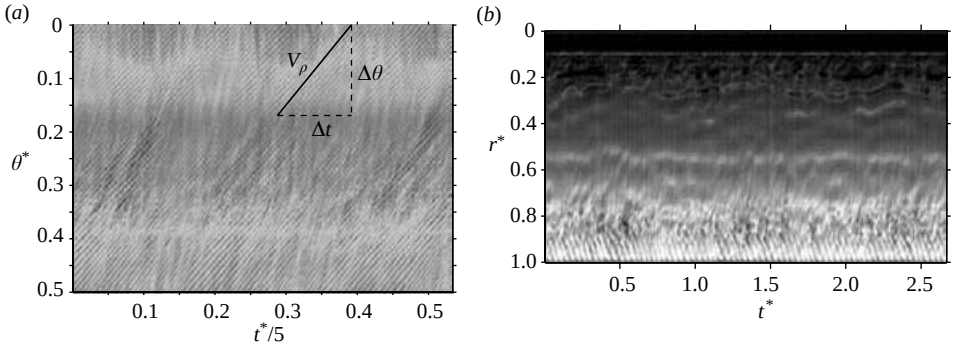

FIGURE 5. Space–time diagram for $Re = 2.05 \times 10^4$ and $V_z = 0.0754$: (*a*) in terms of a fixed half-circle at $r^* = 0.935$, (*b*) in terms of a radius.

discrepancy for the disappearance threshold, which is probably due to the presence of a radial gap j in our experiment. Schouvelier (1998) and Rémy (2004) have shown that this small parameter is predominant for the appearance of instabilities in rotor–stator flows. The SR2 spiral patterns are still observed when a centripetal throughflow is superimposed. The spiral angle is almost the same: $15^\circ \leqslant \epsilon \leqslant 17^\circ$ for $0 \leqslant V_z \leqslant 0.0372$ and $Re = 4.31 \times 10^4$. Two effects should to be noticed: in the case of a strong inward throughflow, the SR2 network exhibits defects due to the axial jet. Secondly, the appearance and disappearance thresholds decrease as the inwardly directed throughflow rises. This can be easily understood by considering a local Reynolds number based on the tangential velocity in the core of the flow at the critical radial location: $Re_{r_c} = K\Omega r_c^2/\nu$, with $K = V_\theta/\Omega r_c$ the ratio between the mean tangential velocity in the core of the flow and that of the disk at the same radius. K is in fact the entrainement coefficient of the fluid. For a given rate of rotation Ω, increasing the axial velocity V_z (throughflow Q), increases K. This means that the critical Reynolds number Re_{r_c} increases too. It explains why the bifurcation leading to these spirals occurs for lower rotational Reynolds numbers Re when the axial velocity V_z is increased.

4. Description of the SRJ2 spiral rolls

Figures 5(*a*) and 5(*b*) represent two space–time diagrams respectively in terms of an angle ($\theta^* = \theta/2\pi$) and in terms of a radius ($r^* = r/R_2$) of the flow for $Re = 2.05 \times 10^4$ and $V_z = 0.0754$. They correspond to the visualization of the SRJ2 spirals in figure 4*a*. We define the dimensionless time as $t^* = 2\pi t/\Omega$. The diagonal lines in figure 5(*a*) correspond to the SRJ2 spiral passing. It enables the phase velocity $V_p = \Delta\theta/\Delta t$ of the structures to be determined. The space–time diagram in terms of a radius (figure 5*b*) shows the critical radial location r_c^* for the appearance of the patterns, as well as their frequency N and their azimuthal wavenumber $k^* = kR_2$, which is also the number of structures by rotation. The inclination angle ϵ of the spirals is also determined from the visualizations. Figure 5(*b*) shows clearly that the SRJ2 network is located at the periphery of the cavity.

Figure 6(*a–d*) shows the main characteristics of the SRJ2 spiral rolls in terms of the axial velocity V_z and to the rotational Reynolds number Re. There is a strong competition between the effects of the rotation (in the tangential direction) and those of the axial throughflow (in the radial direction). Figure 6(*a*) confirms the

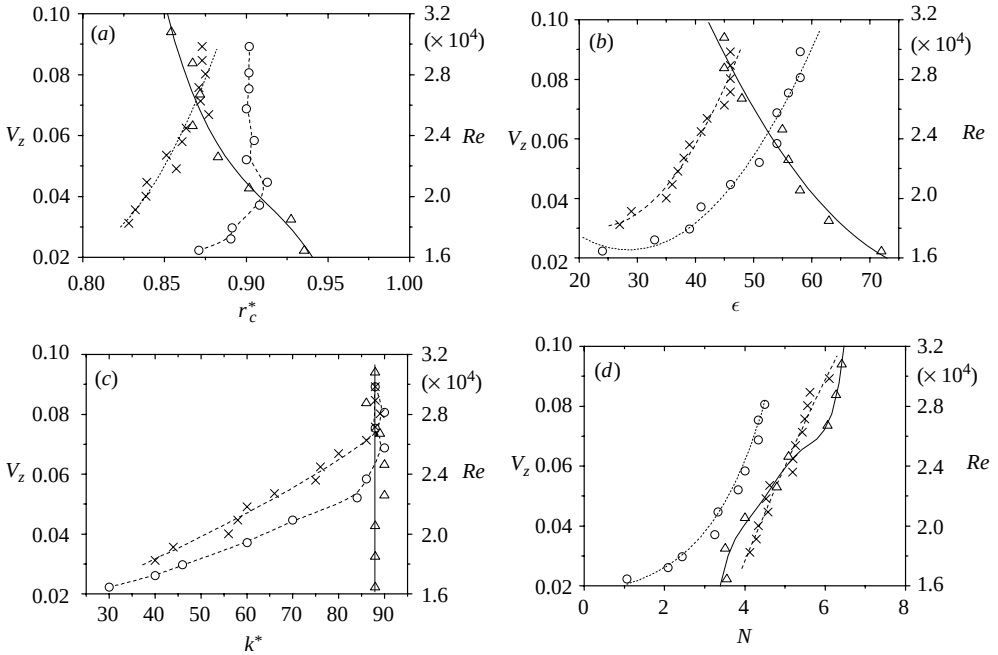

FIGURE 6. Characteristics of SRJ2 spiral rolls in terms of V_z for ○, $Re = 2.05 \times 10^4$ and ×, $Re = 2.87 \times 10^4$ and △, Re for $V_z = 0.0892$: (*a*) critical radius r_c^*, (*b*) inclination angle ϵ, (*c*) azimuthal wavenumber k^*, (*d*) frequency N (Hz).

location of the spiral rolls at the periphery of the rotating disk and shows that the critical radius r_c^* for their appearance depends slightly on the axial velocity V_z and on the Reynolds number Re. The SRJ2 patterns appear for $r_c^* \geqslant 0.82$ in this range of parameters. The value of r_c^* increases with increasing values of V_z or decreasing values of Re. Some velocity measurements using the LDA technique at $r^* = 0.964$ and for different flow parameters (see figure 2 for example) have shown that the spirals are located at $z^* \geqslant 0.35$. This instability is, then, not due to the destabilization of the Ekman boundary layer. We compute the mean field for $Re = 2.5 \times 10^4$ and $V_z = 0.0892$ (figure 9 below) by using the laminar numerical code derived from the Reynolds stress modelling (RSM) of Poncet, Chauve & Schiestel (2005*b*). At the radial location $r^* = 0.919$, figure 9 shows that the flow is of Batchelor type with two separated boundary layers. For $z^* \geqslant 0.4$, the flow is centripetal ($V_r^* < 0$).

For a given Reynolds number $Re = (2.05 - 2.87) \times 10^4$, on increasing the axial velocity V_z, the radial component of the flow increases. As a consequence, the inclination angle ϵ (figure 6*b*) increases too and we observe the development of more and more structures k^* until a threshold $k^* = 90$ is reached (figure 6*c*). On the contrary, for a given axial velocity $V_z = 0.0892$, on increasing the Reynolds number, the tangential component of the flow increases. Consequently, the inclination angle ϵ (figure 6*b*) decreases. The azimuthal wavenumber $k^* \simeq 90$ is fixed by the value of the axial velocity V_z and does not depend on the Reynolds number for this strong inward throughflow (figure 6*c*). On increasing the throughflow V_z or the Reynolds number Re, the entrainment coefficient K of the fluid is increased according to relation (4.1) below. So the tangential velocity of the spirals increases too. This is confirmed in

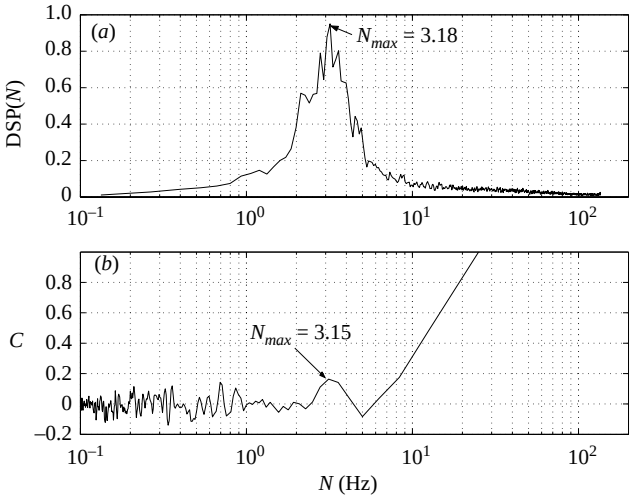

FIGURE 7. Frequency of the SRJ2 spirals for $Re = 2.05 \times 10^4$ and $V_z = 0.0754$ at $r^* = 0.964$: (*a*) power spectral density DSP of the LDA data, (*b*) correlation of the grey density on the space–time diagram (figure 5*b*).

figure 6(*d*). The frequency N is indeed increased by a faster rotation of the disk or a stronger axial jet.

In figure 7, we compare the frequency of the SRJ2 spirals obtained from visualizations and velocity measurements for $Re = 2.05 \times 10^4$ and $V_z = 0.0754$ at the point ($r^* = 0.964$, $z^* = 0.567$). We first calculate the power spectral density (DSP) of the LDA data in terms of the frequency N (Hz) (figure 7*a*): the maximum frequency $N_{max} = 3.18$ Hz is the frequency of the SRJ2 spiral rolls. To validate this result, we have also calculated the correlation C of the grey density from the space–time diagram (figure 5*b*) at the line $r^* = 0.964$. The first frequency peak (figure 7b) corresponds to the frequency of the structures $N_{max} = 3.15$ Hz. There is, then, an excellent agreement between these two methods: the frequency of the SRJ2 patterns for $Re = 2.05 \times 10^4$ and $V_z = 0.0754$ is the same to within less than 1 %. This result is very satisfactory because the visualizations give integrated values in the axial direction z, whereas the LDA technique provides one-point measurements.

For a given axial velocity $V_z = 0.0829$, we have compared the phase velocity V_p of the SRJ2 spirals to a mean velocity $V_f = 0.5K\Omega r_c$ at the periphery of the cavity for different Reynolds numbers (figure 8). V_f is the average of the mean tangential velocity $V_\theta(r_c) = K\Omega r_c$ in the core of the flow at the critical radial location and that at the shroud $V_\theta(R_3) = 0$. To determine the entrainment coefficient K of the fluid, we have extended, to the case of laminar flows, the law obtained by Poncet, Chauve & Le Gal (2005*a*) with the following friction coefficient: $C_f = 1.328 \times Re^{-1/2}$ (Schlichting 1960). Finally, we obtain the following relation:

$$K = 0.41 + 0.88 Cq_{lam} \tag{4.1}$$

where $Cq_{lam} = QRe_r^{1/3}/(2\pi\Omega r^{10/3})$ is a local flow rate coefficient. As shown in figure 8, the two velocities V_p and V_f are comparable but the phase velocity V_p is slightly weaker than the mean tangential velocity V_f of the fluid especially for the highest values of the Reynolds number. Even though there is always a shear stress between the shroud and the core of the flow, it seems not to lead to the formation of these

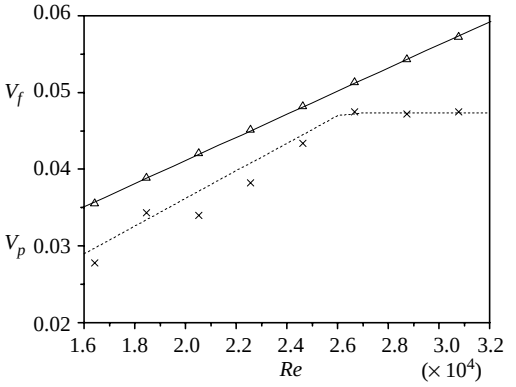

FIGURE 8. Phase velocity V_p ($\times$) of the SRJ2 spirals compared to the mean tangential velocity V_f ($\triangle$) at the periphery of the cavity for $V_z = 0.0829$ and different Reynolds numbers.

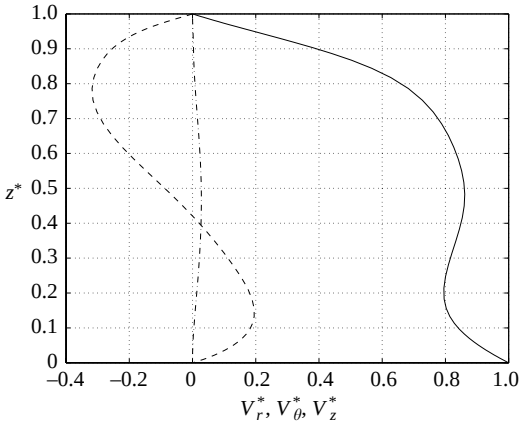

FIGURE 9. Mean velocity profiles for $V_z = 0.0829$ and $Re = 2.5 \times 10^4$ at $r^* = 0.919$ (RSM model): ——, radial component $V_r^* = V_r/(\Omega r)$; —, tangential component $V_\theta^* = V_\theta/(\Omega r)$, —·—, axial component $V_z^* = V_z/(\Omega r)$.

spiral patterns. We conclude that the SRJ2 spiral rolls rotate at a rate lower than the fluid.

For a weak inward throughflow, the characteristics of the spiral rolls are comparable with the SR1 network observed by Schouvelier *et al.* (2001). The flow is then mainly governed by the rotation. For high values of the axial velocity V_z, the flow is governed by the throughflow and the SRJ2 patterns are comparable to the structures denoted 2 by Rémy (2004) and Rémy *et al.* (2005). The main characteristics of structures 2 are a high wavenumber $40 \leqslant k^* \leqslant 70$ and a weak frequency $N \leqslant 3.5$ Hz. We recall also that they are located at the periphery of the rotating disk. Rémy *et al.* (2005) proved that this instability is a crossflow instability: an azimuthal flow due to the rotation is in competition with a radial flow due to the inward throughflow and the radial profiles of the axial and azimuthal velocities exhibit inflection points. That is also the case for the SRJ2 spirals. Figure 9 confirms that an azimuthal flow is in competition with an radial inflow (the axial component is quasi-zero) and that the mean velocity profiles also exhibit inflection points. The SRJ2 spirals are thus alos due to a crossflow instability.

5. Conclusion

We have studied experimentally the intermediate-aspect-ratio ($G = 0.0429$) instabilities, which develop in a rotor-stator cavity when an axial inward throughflow is superimposed. We performed both visualizations and velocity measurements using a two-component LDA technique. Two instabilities appear as spiral rolls: the SR2 network observed by Schouvelier *et al.* (2001) and a new instability denoted SRJ2, which is located at the periphery of the cavity and attached to the shroud. This instability is in fact a crossflow instability: an azimuthal flow due to the rotation is in competition with the radial flow due to the inward throughflow. Moreover we showed that the mean radial and tangential velocity profiles exhibit inflection points, which is a characteristic of this type of instability. We have also shown that the SRJ2 spiral rolls are comparable to the structures denoted 2 by Rémy *et al.* (2005), which are a crossflow instability attached to the axial jet: spirals with a small wavelength and a large wavenumber. The only discrepancy remains the inclination angle, which is much larger in our experiment, up to 72°, which could be due to the radial gap.

The authors wish to thank M. Amielh for helpful comments during the LDA measurements.

REFERENCES

Cousin-Rittemard, N., Daube, O. & Le Quéré, P. 1998 Sur la nature de la première bifurcation des écoulements interdisques. *C.R. Acad. Sci. Paris* IIb **326**, 359–366.

Cros, A. & Le Gal, P. 2002 Spatiotemporal intermittency in the torsional couette flow between a rotating and a stationary disk. *Phys. Fluids* **14**, 3755–3765.

Gauthier, G., Gondret, P. & Rabaud, M. 1999 Axisymmetric propagating vortices in the flow between a stationary and a rotating disk enclosed by a cylinder. *J. Fluid Mech.* **386**, 105–126.

Piétry, L. 1997 Etude expérimentale de jets turbulents axisymétriques à densité variable. Analyse des propriétés statistiques des échelles du champ dynamique. PhD thesis, Université d'Aix-Marseille II.

Poncet, S., Chauve, M.-P. & Le Gal, P. 2005*a* Turbulent rotating disk flow with inward throughflow. *J. Fluid Mech.* **522**, 253–262.

Poncet, S., Chauve, M.-P. & Schiestel, R. 2005*b* Batchelor versus stewartson flow structures in a rotor-stator cavity with throughflow. *Phys. Fluids* **17**, 075110.

Rémy, D. 2004 Etude expérimentale par la tomographie et la PIV des structures instationnaires dans une cavité rotor-stator avec aspiration. PhD thesis, Université des Sciences et Technologies de Lille.

Rémy, D., Gauthier, G. & Buisine, D. 2005 Instabilities between rotating and stationary parallel disks with suction. *Phys. Fluids* **17**, 018102.

Schlichting, H. 1960 *Boundary-layer Theory*, 7th Edn. McGraw-Hill.

Schouvelier, L. 1998 Sur les instabilités des écoulements entre un disque fixe et un disque en rotation. PhD thesis, Université d'Aix-Marseille II.

Schouvelier, L., Le Gal, P. & Chauve, M.-P. 2001 Instabilities of the flow between a rotating and a stationnary disk. *J. Fluid Mech.* **443**, 329–350.

Serre, E., Crespo del Arco, E. & Bontoux, P. 2001 Annular and spiral patterns in a flow between a rotating and a stationary disk. *J. Fluid Mech.* **434**, 65–100.